TROPESS Level 2 Algorithm Theoretical Basis Document (ATBD) V1

Kevin W. Bowman
John R. Worden
Robert Herman
Vivienne H. Payne
Vijay Natraj
Karen Cady-Peirera
Helen Worden

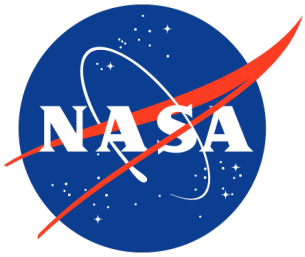

TROPESS ATBD V1

Prepared for
NASA

Kevin W. Bowman[1], John Worden[1], Robert Herman[1], Karen Cady-Pereira[2], Vijay Natraj[1], Vivienne H. Payne[1], Helen Worden[3], Susan Kulawik[4]
[1]*NASA Jet Propulsion Laboratory*
[2]*Atmospheric Environmental Research*
[3]*National Center for Atmospheric Research*
[4]*BAER Institute*

Jet Propulsion Laboratory, California Institute of Technology

The research was carried out at the Jet Propulsion Laboratory, California Institute of Technology, under a contract with the National Aeronautics and Space Administration (80NM0018D0004)

Table of Contents

List of Tables

List of Figures

1. Introduction

1.1 Purpose

This Algorithm Theoretical Basis Document (ATBD) describes the algorithmic underpinning of atmospheric retrievals and ancillary products in the TRoposphericOzone and its Precursors from Earth System Sounding (TROPESS) Level 2 Standard Data Products. These products are archived at the NASA Goddard Earth Science Data and Information Services Center (GES DISC) Distributed Active Archive Center (DAAC) (https://disc.gsfc.nasa.gov). The TROPESS standard products consist of vertical volume mixing ratio profiles of trace gases (e.g., O_3, carbon monoxide), physical variables (e.g., temperature, water vapor, cloud optical depth), and ancillary quantities (e.g., emissivity). These products are generated from multiple instruments and their combinations. The conceptual framework for the algorithms are based around optimal estimation (*Rodgers*, 2000). The algorithm has substantial heritage from the Tropospheric Emission Spectrometer (TES; *Beer*, 2006; *Bowman et al.*, 2006) but has evolved into the MUlti-SpEctra, MUlti-SpEcies, Multi-SEnsors (MUSES) algorithm (*Fu et al.*, 2016). The MUSES algorithm combines radiance measurements from multiple wavelengths from the thermal infrared to the ultraviolet to estimate these L2 products with degrees of freedom for signal (DOFS) (see Sec. 3.6) greater than could be obtained by any single wavelength region. These radiances can be obtained from multiple instruments. The MUSES algorithm builds on pioneering work to combine TES and the Ozone Monitoring Instrument (OMI), which has resulted in a substantial body of literature that documents these algorithms (*Fu et al.*, 2013; *Worden et al.*, 2007b). The purpose of this document is to not only introduce these algorithms but also navigate the relevant literature.

1.2 Scope

This document covers the algorithm theoretical basis for the parameters derived from the MUSES algorithm to be included in the TROPESS Level 2 Data Products. On-going development and prototyping efforts may result in modifications to parts of certain algorithms. This ATBD will be updated in the future accordingly.

1.3 Applicable Documents

Table 1. Reference Documents

Document	Purpose
CrIS Algorithm Theoretical Basis Document (L1B) (CrIS SDR, CrIS L1B ATBD)	Presents a detailed description of the NASA L1B algorithm. The spectral radiances produced from this algorithm are ingested into the MUSES L2 algorithm
OMI Algorithm Theoretical Basis Document, Volume I: OMI Instrument, Level 0-1b processor, Calibration & Operations, Version 1.1, ATBD-OMI-01, August 2002.	Contains a general description of the OMI instrument and its measurement modes, and describes in detail the OMI Level 0 to 1B processing algorithms that convert instrument counts to calibrated radiances, ground and in-flight calibration, and the flight operations needed to collect science data.
OMI Algorithm Theoretical Basis Document, Volume III: Clouds, Aerosols, and Surface UV Irradiance, Version 2.0, ATBD-OMI-03, August 2002.	Presents OMI retrieval algorithms for producing the aerosols, clouds, and surface UV radiation products
AIRS Algorithm Theoretical Basis Document, Level 1B, Part 1: Infrared Spectrometer, Version 2.2i, Nov 2000.	Presents a detailed description of the NASA AIRS L1B. The spectral radiances produced from this algorithm are ingested into the MUSES L2 algorithm.
Algorithm theoretical basis document for the TROPOMI L01b data processor, Issue 8.0.0, June, 2017.	Contains the description of the Level-0 to Level-1b data processing for the TROPOMI mission.

1.4 Revision History

This is the initial verion (1.0). Subsequent version will be updated here.

2. Background

2.1 Project Overview

Tropospheric sounding from satellite observations provides critical information about atmospheric composition and its impact on human health and climate. The TRopospheric Ozone and Precursors from Earth System Sounding (TROPESS) project will generate Earth System Data Records (ESDRs) of ozone and other atmospheric constituents by processing data from multiple satellites through a common retrieval algorithm and processing system. These products will be validated using uncertainty analysis in conjunction with independent measurements. These steps will characterize the accuracies needed to make long-term trends through multi-satellite records and chemical data assimilation. Scientific analysis

and evaluation leading to peer-reviewed publications will demonstrate the scientific value of these ESDRs and their utility to the broader community. The science team will contribute to international initiatives such as the Tropospheric Ozone Assessment Report.

The TROPESS activity leverages innovations at JPL pioneered by the Tropospheric Emission Spectrometer (TES) team in combining data from multiple satellites to form a common retrieval framework, which is known as the MUlti-SpEctra, MUlti-SpEcies, Multi-SEnsors (MUSES) science data processing system (MUSES-SDPS). This framework will be applied to a combined suite of hyperspectral thermal infrared, near-infrared, and ultraviolet instruments to generate Earth System Data Records (ESDRs) of Earth's tropospheric composition, including ozone (O_3) , carbon monoxide (CO), methane (CH_4), and deuterated water vapor (HDO). These ESDRs will have DOFS (Eq. 8) superior to composition measurements derived from any single instrument. These data will be based on optimal estimation retrievals, which include critical diagnostics such as observation operators and uncertainty metrics sufficient for assimilation into Earth system models (Sec. 3.6 and 3.7).

TROPESS will produce 3 streams of data: (1) Forward Stream (2) Renalysis Stream (3) Special collections. The forward stream provides low-latency multi-instrument and single-instrument products with a latency less than one week. The reanalysis stream uses a common retrieval algorithm version to produce a multidecadal record. The third stream–"special collections"–are provided on an as-needed and as-available basis to support NASA field missions and individual-investigator requests over specific regions, e.g., large wildfires.

Table 2 shows the instruments that will be processed by TROPESS. The input version will change with new updates and will be reflected in the TROPESS output products. Table 3 shows an example of products for each configuration, e.g., six distinct O_3 products. All products for single instrument retrievals will also be included in joint products, e.g., CrIS NH_3 will be in CrIS+TROPOMI products. Where joint products are explicitly noted, the product will have different accuracy, precision and vertical sensitivity than single-instrument products. All products will include observation operators and uncertainty estimates to enable ingestion into data assimilation systems and comparisons with other data sets (Sec. 3.7). Data products will be accompanied by a data user's guide, which includes a validation statement. The species delivered will be temperature, water vapor, O_3, carbon monoxide, O_3, HDO, methane, PAN, methanol, NH_3, instantaneous radiative kernels. Isoprene will be provided on a best-effort basis.

2.2 Level 2 Products

The TROPESS L2 data products, and their L1B data sources are shown in Tables 1 and 2. TROPESS will produce Forward Streams and Reanalysis Streams for two instrument pairs: AIRS+OMI and CrIS+TROPOMI. These include single-instrument along with instrument combinations.

Table 2. Instruments, input data, and sources used for TROPESS processing

TROPESS Data Stream	Instrument	Input Datasets	Source
AIRS+OMI	AIRS	AIRIBRAD_005	AIRS L1B
	OMI	OML1BRUG_003	OMI L1B
	OMI	OMCLDO2_003	OMI Cloud
CrIS+TROPOMI	CrIS	SNPPCrISL1B_2	CrIS L1B
	TROPOMI	S5P_L1B_IR_UVN	TROPOMI L1B
	TROPOMI	S5P_L1B_IR_SIR	TROPOMI L1B NIR

2.3 Instrument Description and Characteristics

Table 2 shows the multiple L1B input data datasets used to generate TROPESS products from each data stream. For the forward stream, the updated versions of the inputs will be incorporated as they become available. The reanalysis stream, however, will use the same input versions throughout the record.

2.4 AIRS+OMI Stream

The TROPESS L2 AIRS+OMI data stream uses the L1B data from the Atmospheric Infrared Sounder (AIRS) high spectral resolution IR spectrometer, and Level 1B and Level 2 Cloud data from the Ozone Monitoring Instrument (OMI) as inputs.

The Atmospheric Infrared Sounder (AIRS) is a high-resolution thermal IR grating spectrometer onboard the Aqua platform in afternoon orbit. A description of the instrument and objectives can be found here and at https:\airs.jpl.nasa.gov. The accuracy, precision, and processing algorithm are discussed in the AIRS L1B ATBD.

The Ozone Monitoring Instrument (OMI) is a high-resolution UV-Vis grating spectrometer onboard the Aura platform in an afternoon orbit. An overview of the instrument and objectives can be found at the OMI website. The precision and accuracy of the OMI data are described in the OMI L1B ATBD (ATBD-OMI-01 and ATBD-OMI-03, respectively).

2.5 CrIS+TROPOMI Data Stream

The TROPESS L2 CrIS+TROPOMI data stream uses L1B data from the Cross-track Infrared Sounder (CrIS) and TROPOspheric Monitoring Instrument (TROPOMI) as inputs.

The Cross-track Infrared Sounder (CrIS) is a Fourier Transform Spectrometer (FTS) onboard the Suomi National Polar-Orbiting Partnership (SNPP) satellite, which launched on October 28, 2011. CrIS is a flat-mirror Michelson interferometer that measures interferograms in three Infrared (IR) bands simultaneously. The CrIS L1B data product consists of calibrated radiance spectra and geolocation information, metadata and various derived parameters related to the observations. The MUSES can be applied to CrIS instruments on

the other Joint Polar Satellite System (JPSS) instruments. This application will be explored in the future.

The TROPOspheric Monitoring Instrument (TROPOMI) consists of a spectrometer with spectral bands in the ultraviolet, the visible, the near-infrared and the shortwave infrared. TROPOMI launched on October 13, 2017 on the Copernicus Sentinel-5 Precursor satellite (S5p) and was jointly developed by The Netherlands and ESA. The TROPESS L2 products use the L1B data from both the UV and NIR channels. More information can be found at the TROPOMI website.

2.6 Species

The primary atmospheric species to be delivered are described in Table 3: ozone (O3), carbon monoxide (CO), and temperature (TATM), methane (CH4), deuterated water (HDO), peroxyacetyl nitrate (PAN), and ammonia (NH3). Subsequent releases will include Ozone Instantaneous Radiative Kernels (O3 IRKs), Methanol, and (best-effort) Isoprene (ISOP). The sub-stream column refers to the L1B instrument radiances that are used in each product. Every check box in the table represents a product. For example, there are six unique O_3 product, including three O_3 products from the AIRS+OMI data stream (AIRS+OMI, OMI, and AIRS), and three O_3 products from the CrIS+TROPOMI data stream (CrIS+TROPOMI, CrIS, and TROPOMI). Species labelled as $*^1$ in Table 3 indicate they are expected to be included as part of later deliveries. Species with superscript $*^2$ are pursued on a best-effort basis. Additional species may be included on a best-effort basis depending on availability from separately funded projects, as part of the TROPESS Special Collections.

3. Algorithm Description

3.1 Algorithm Overview

The MUSES Level 2 processing system is shown in Fig. 1. Calibrated L1B spectral radiances from a number of different satellites are ingested into MUSES where they are geolocated with respect to each other. These geolocated radiances are then passed to the Retrieval Program Generation Executable (PGE). The Retrieval PGE can be broken down into 3 components: (1) Strategy, (2) Retrieval, and (3) Error Analysis. The Strategy executes a sequence of Retrievals. The retrieved state from one step is then passed to a subsequent step where additional parameters are retrieved. For example, meteorological variables like temperature, water vapor, and clouds may be estimated first, and then other parameters such as methane or carbon monoxide are computed afterwards. Breaking the retrieval down into steps mitigates against nonlinearities in the retrieval process, relative radiance impacts of some parameters (e.g., temperature vs. minor gases), and stiffness in the optimization process, i.e., the difficulty in computing a minimum. The Retrieval uses forward models, which generates synthetic spectral radiances, configured for each satellite measurement, error specification for both the measurement and state, and a nonlinear optimization code that minimizes the difference between observed and predicted radiances

Table 3. Retrieval products for different configurations of the AIR+OMI and CrIS+TROPOMI data stream under forward stream (FS) and reanalysis stream (RS).

Stream				Atmosphere Species									
Data stream	Processing Strategy	Sub-stream	Day/ Night Cover-age	O_3	CO	TATM	HDO/ H_2O	CH4	NH3	PAN	O3 IRK	Meth	Isop
AIRS +OMI	FS, RS	AIRS +OMI	Daytime Only	*									
		OMI	Daytime Only	*									
		AIRS	Daytime /Night-ime	*	*	*	*	*	*	*	*1		
CrIS + TROPOMI	FS, RS	CrIS + TROPOMI	Daytime Only	*	*		*	*			*		
		TROPOMI	Daytime Only	*	*		*	*					
		CrIS	Daytime Only	*	*	*	*	*	*	*	*1	*1	*2

subject to second-order statistical knowledge of the state. The last step is the Error Analysis that computes posterior error covariances and averaging kernels. These may be used passed to subsequent retrievals as determined by the retrieval Strategy. Once completed, the retrieved values and their uncertainties along with diagnostics are stored in output files and then delivered for permanent storage.

3.2 Introduction

One of the motivations of the TROPESS project is shown in Figure 2. Thermal infrared instruments like TES measure between roughly 4-15.4 microns (650-2500 cm^{-1}) whereas instruments such as TROPOMI measure in the near infrared and ultraviolet at wavelengths less than 2 microns. However, molecular absorption for the same molecule can occur at multiple spectral regions. For example, O_3 absorbs both in the thermal 10 micron band as well as the ultraviolet 0.3 micron band. Consequently, retrieving O_3 from both spectral bands provides an opportunity to combine all the available information (*Fu et al.*, 2013, 2016, 2018; *Worden et al.*, 2007b).

Optimal estimation provides a framework for assessing the information content of radiance bands and their combinations (*Rodgers*, 2000). Consequently, it is conceptually straightforward to extend the methods to incorporate panspectral measurements, i.e., multiple spectral bands acting primarily through emission as well as those acting through re-

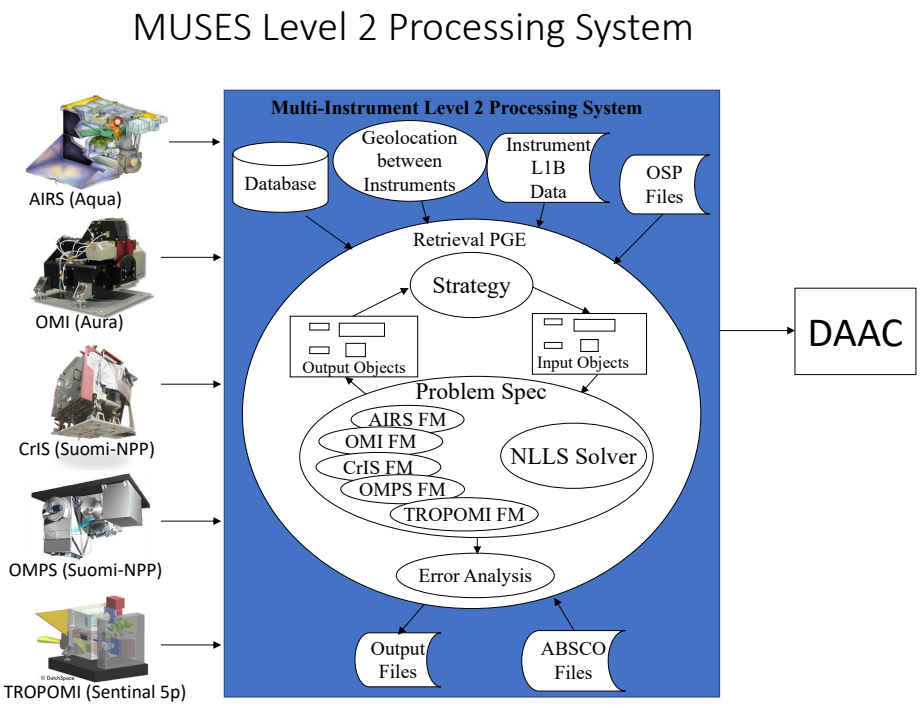

Fig. 1. Overview of MUSES Processing

flection. The technical challenges are related to the forward model physics needed to accurately simulate different bands, the consistency of spectroscopic input, calibration, and the necessary atmospheric and surface state parameters.

3.3 Forward Model

The forward model, denoted as $\mathbf{L}(\mathbf{x}) : \mathbb{R}^n \longrightarrow \mathbb{R}^m$, projects an atmospheric (and surface) state, denoted by $\mathbf{x}$, to measurements for a particular instrument. These measurements account for the radiative transfer through the atmosphere, the geometry between the atmosphere and the instrument, and the characteristics of the instrument. The latter includes the instrument line shape (ILS), which accounts for the spectral response to a hypothetical monochromatic radiance at one wavelength. Fourier Transform Spectrometers typically have one ILS for all frequencies (*Beer*, 1992) but must account for the optical geometry of the detector (*Bowman et al.*, 2000). Grating spectrometers, on the other hand, have an instrument line-shape for each detector element in a grating (e.g., *Lee et al.*, 2017).

3.3.1 Thermal Infrared Radiative Transfer

The basis for the thermal infrared (TIR) radiative transfer model can be found in *Clough et al.* (2006). This analytic methdology for calculating the radiative transfer from a "line-by-line" approach has been updated to use a more computationally efficient approach called

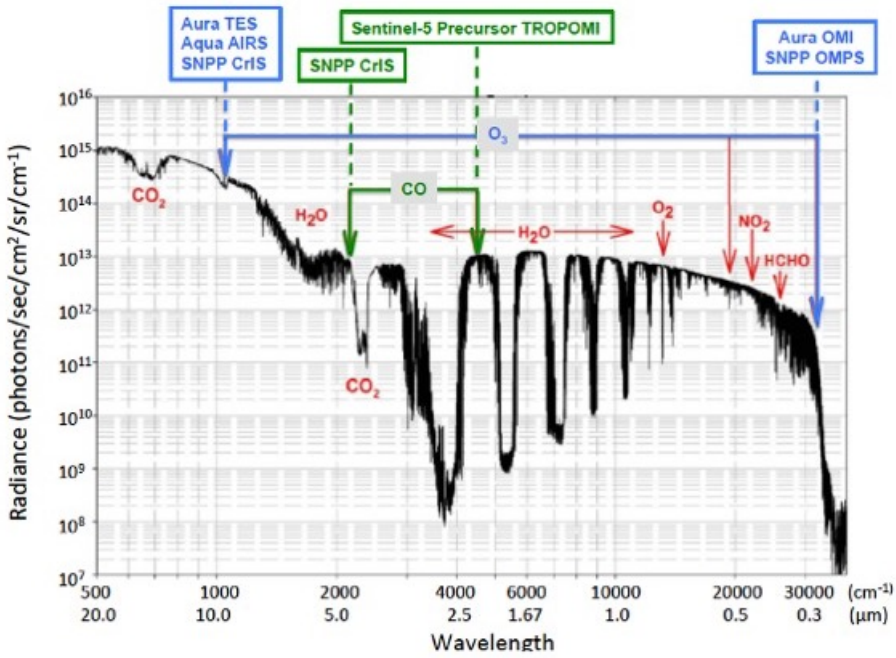

Fig. 2. Outgoing radiance from 0.3-20 microns. Molecular absorption features are shown in red. Instruments are designed to measure over limited spectral bands and are noted in blue and green.

Optimal Spectral Sampling (OSS, *Moncet et al.*, 2008, 2015). The radiative transfer code includes a simplified cloud forward model (*Eldering et al.*, 2008; *Kulawik et al.*, 2006a) that uses a single layer, gray body model for approximating the radiative transfer through clouds.

The propagation of radiation through the atmosphere is determined by raytracing for both nadir and off-nadir angles. The approach builds off the TES heritage described in the TES Level 2 ATBD.

3.3.2 Ultraviolet/Shortwave Infrared Radiative Tranfser

Radiative transfer (RT) calculations in the ultraviolet (UV) spectral region use the VLIDORT model (*Spurr*, 2008, 2006) for the numerical computation of the Stokes vector, and its Jacobians with respect to atmospheric trace gas concentrations and surface properties. We follow the basic methodology outlined in *Liu et al.* (2010a). A single scattering model (*Sioris and Evans*, 2000) is used to simulate the Ring effect. Radiances are calculated for a Rayleigh atmosphere (no aerosols) with a Lambertian underlying surface. We use a surface reflectance climatology constructed using three years of OMI measurements obtained between 2004 and 2007 (*Kleipool et al.*, 2008). A constant surface albedo is assumed in the (OMI) UV-1 band. The surface albedo in the (OMI) UV-2 band is wavelength-dependent and is represented as a first-order polynomial, which also partly accounts for the effects of aerosols. Although higher-order polynomials can further reduce fitting residuals, they

adversely impact retrieval accuracy due to overly strong correlation with O_3. In the spectral regions of interest, atmospheric SO_2 and BrO absorption are typically much weaker than that of O_3, and are hence not modeled or retrieved, although this can be easily modified. High-resolution (0.01 nm) O_3 cross sections (*Brion et al.*, 1993) are used in the simulations; this data set has been found to significantly reduce fitting residuals in the Huggins band compared to other cross section data sets (*Liu et al.*, 2007). Temperature dependence of O_3 absorption is accounted for by using temperature profiles from TROPESS TIR products. Clouds are treated as reflecting boundaries with a Lambertian reflectance of 0.8. Radiance calibration factors are applied to the calculated radiances.

Recent work has focused on improving the computational efficiency of the RT model, as well as extension to the shortwave infrared (SWIR) spectral region, utilizing an optical property-based principal component analysis (O-PCA) technique. O-PCA reduces the high computational cost of RT calculations by taking advantage of redundancies in both the angular (number of computational quadrature angles ("streams") for discretizing the RT problem at a single monochromatic wavelength) and spectral (number of monochromatic wavelengths for which RT calculations are performed) dimensions. Reduction of the number of streams with almost no loss of accuracy is based on two fundamental principles: (1) separation of single and multiple scattering contributions (*Duan et al.*, 2005), and (2) correlation between multi-stream and two-stream calculations for the multiple scattering contribution (*Natraj et al.*, 2005). O-PCA computes an approximate radiation field I_{PCA} at wavelength λ in the following manner:

$$I_{PCA}(\lambda) = I_{2S}(\lambda)C(\lambda) + I_{FO}(\lambda) \tag{1}$$

The subscripts 2S and FO stand for the two-stream and single scattering approximations to the radiance. C is a correction factor computed using the O-PCA technique.

Wavelength optimization is performed using a three-step procedure: binning, eigenvalue problem solution and radiance back-mapping. Each bin is characterized by grouping certain optical properties (such as atmospheric layer trace gas optical depth values or single scattering albedos) that are similar within the bin. The selection for spectral binning is often based on the division of (the logarithms of) the total-atmosphere gas optical depths into decadal intervals (e.g., *Natraj et al.*, 2010) . These bins could also be further divided by splitting along the median scattering optical depth (*Kopparla et al.*, 2016) . A wide variety of binning schemes were explored by *Kopparla et al.* (2017); we use the optimal scheme described therein.

O-PCA exploits redundancy in a binned data set of optical properties by expressing the variance of this data set in terms of the first few principal components (PCs). In practice we use the set of mean-removed optical property logarithms. Usage of logarithms is for computational efficiency reasons (e.g., *Natraj et al.*, 2005). If the data set is strongly correlated (as is the case for narrow spectral bands of the kinds used by TROPESS), most of the optical information will be contained in the first few PCs (those with the largest eigenvalues). Together with the mean, these PCs define a much smaller set of PCA-projected optical states. The key to O-PCA performance enhancement is to carry out fully accurate

multiple scattering RT simulations only for this reduced set of optical states, instead of performing time-consuming calculations at every spectral point in the bin. We use the fast 2S model (*Spurr and Natraj*, 2011) to approximate the multiple scattering contribution at each spectral point, and then develop correction factors based on RT calculations for the PCA-projected optical states. This correction applies only to the multiple scatter field; single scatter calculations are always performed accurately at full spectral resolution.

The eigenvalue problem solution is done for data sets that are logarithms of optical properties, and the radiation-field restoration likewise uses log-space. The use of logarithms for the intensity calculation offers two advantages: negative intensities are automatically avoided, and the fact that extinction is exponential in the absence of scattering is taken into account. We use the PC scores (projections of the original data set of optical properties on to the PCs) for radiance restoration. The restoration is based on the assumption that, for all wavelengths in the given bin, the difference between the logarithm of the accurate (multiple scatter) radiance field and the approximate (2S) field can be derived from the PCA-projected RT results and a second-order central-difference expansion in terms of the PC scores. Details of the procedure, as well as its linearization, can be found in *Spurr et al.* (2013).

3.4 Retrieval

The retrieval methodology is built on optimal estimation (OE), which is the basis of the TES and TROPESS retrieval algorithms (*Bowman et al.*, 2006). Given spectral radiance observations, $\mathbf{y} \in \mathbb{R}^M$ (where M is the number of spectral points), from possibly multiple instruments, the objective of the retrieval is to determine an atmospheric state, $\mathbf{x} \in \mathbb{R}^N$ (where N is the number of atmospheric parameters), that is consistent with those observations through the forward model $\mathbf{L}(\mathbf{x}) : \mathbb{R}^N \longrightarrow \mathbb{R}^M$. However, the observations are imprecise. The additive noise model relates the observations to the atmospheric state through the following *Bowman et al.* (2006)

$$\mathbf{y} = \mathbf{L}(\mathbf{x}, \mathbf{b}) + \boldsymbol{\varepsilon} \tag{2}$$

where $\mathbf{b}$ represents non-retrieved parameters such a spectroscopy and $\boldsymbol{\varepsilon}$ is random noise where $E[\boldsymbol{\varepsilon}] = 0$ and $\mathbf{S}_\varepsilon = E[\boldsymbol{\varepsilon}\boldsymbol{\varepsilon}^\top]$ is the measurement error covariance. However, there may be multiple atmospheric states that can represent the observations. From this standpoint, the retrieval is considered an ill-posed problem (*Tarantola*, 2005). An ill-posed problem can be transformed into a well-posed problem through two different approaches. The first is based upon "hard constraints", which map the full atmospheric state vector to a smaller space or basis set. The most straight-forward implementation is reducing the number of levels and performing interpolation. This reduced state is called the *retrieval vector*, $\mathbf{z}$. The relationship between the full state vector and the retrieval vector is computed through a mapping matrix

$$\mathbf{x} = \mathbf{M}\mathbf{z}. \tag{3}$$

The second approach is based upon "soft" constraints, i.e., a priori statistical knowledge of the solution space for $\mathbf{x}$ or $\mathbf{z}$.

In an OE framework, both of these approaches are combined in a *maximum a posteriori* (MAP) method, which computes the minimum of the following:

$$C(\mathbf{z}) = ||\mathbf{y} - \mathbf{L}(\mathbf{M}\mathbf{z}, \mathbf{b})||^2_{\mathbf{S}_\varepsilon^{-1}} + ||\mathbf{z} - \mathbf{z}_a||^2_{\Lambda^{-1}} \tag{4}$$

where $\mathbf{z}_a$ is the a priori state vector ($\mathbf{z}_a = E[\mathbf{z}]$). In general $\Lambda = \mathbf{S}_a^{-1}$ where $\mathbf{S}_a = E[(\mathbf{z} - \mathbf{z}_a)(\mathbf{z} - \mathbf{z}_a)^\top]$ is the a prior covariance matrix. These "hard" and "soft" a priori information regularizes the retrieval problem providing a well-posed solution for the minimum in Eq. 4

$$\hat{\mathbf{z}} = \min_{\mathbf{z}} C(\mathbf{z}) \tag{5}$$

The minimization scheme to calculate Eq. 5 is based on nonlinear least-squares techniques (NLLS). The Moré algorithm, which implements a trust-region Levenberg-Marquard algorithm, is the standard approach for TROPESS products (*Bowman et al.*, 2006). The full state vector, $\mathbf{x}$, is used to calculate the radiative transfer, $\mathbf{L}(\mathbf{x}, \mathbf{b})$.

The minimization in Eq. 5 is with respect to $\mathbf{z}$ rather than $\mathbf{x}$, leading to $\hat{\mathbf{z}}$. The constraint vector and matrix are similarly calculated on $\mathbf{z}$. While the minimization is performed with respect to $\mathbf{z}$, the error analysis can be performed on the full state vector. An important nuance is the calculation of the a priori constraints. For practical purposes, these may be modeled and adjusted for better performance than what would be achieved from a sample covariance calculation (*Kulawik et al.*, 2006b).

The interested reader is referred to *Bowman et al.* (2006) for additional details.

3.5 Retrieval configuration

While the overall methodology of optimal estimation is common for all retrievals in Sec. 3.4, specific strategies vary between atmospheric variables. In particular, the retrieved quantity $\hat{\mathbf{x}}$ in Eq. 6 can be either volume mixing ratio (VMR) or the logarithm of VMR. The averaging kernel (Eq. 7) and other error terms will carry the same units.

The initial guess, $\mathbf{z}_0$ (the initial value in the minimization in Eq. 5) and constraint values, $\mathbf{z}_a$, are distributed primarily in latitude, longitude, and month. The initial guess profiles are gridded and generated from model outputs. While the constraint vector and initial guess are play distinct roles in the retrieval, they are generally the same.

In the thermal infrared, initially a brightness temperature (BT) comparison is done to assess the presence of clouds (unexpectedly low BT) or an unexpectedly hot surface (unexpectedly high BT), and an initial guess refinement of clouds and surface temperature may be performed (*Kulawik et al.*, 2006a). In the UV, the cloud fraction is retrieved prior to retrieving O_3. Following the initial guess refinement, a series of steps are done, as specified by the strategy table. In the case of a minor species, like PAN (Sec. 3.5.7), a pre-step is done to retrieve emissivity and cloud properties around the active spectral region, then PAN is retrieved in the active spectral region.

3.5.1 Thermodynamic variables

Thermodynamic variables including H_2O, atmospheric temperature (TATM) and surface temperature (TSUR) are retrieved from both AIRS and CrIS radiances. The algorithm for retrievals of H2O from single footprint AIRS radiances is described in *Worden et al.* (2012, 2019). H_2O is jointly retrieved with HDO, N_2O, CH_4, O_3, Tatm, TSUR, clouds, and emissivity (for land observations) for windows between 671 and 1317 cm^{-1}, with some regions excluded. Validation of AIRS H_2O against reference aircraft profiles is described in the supplement to *Herman et al.* (2020). Prior information for H_2O, TATM and TSUR comes from the Goddard Earth Observing System (GEOS) data assimilation system GEOS-IT (*Gelaro et al.*, 2017) produced by the NASA Global Modeling and Assimilation Office (GMAO). Expected error for TATM is approximately 0.5 K. Validation of TATM is performed against radiosondes. The emissivity is derived from *Seemann et al.* (2008).

3.5.2 Ozone (O_3)

As shown in Fig. 2, O_3 is radiatively active both in the thermal infrared, visible, and ultraviolet bands. Similar to TES, CrIS and AIRS O3 TIR retrievals are performed between 980-1320 cm^{-1} (*Fu et al.*, 2018). In the UV, the O_3 absorption features are found in the Hartley and Huggins bands at 270-310 nm (stratosphere) and 310-330 nm (troposphere). The approach to retrieve O_3 in the UV follows the OE approach in *Liu et al.* (2010b) and extended to OMPS (*Bak et al.*, 2017). O_3 is jointly retrieved with other parameters including temperature, water vapor, HDO, TSUR, cloud, cloud fraction. These strategy follows the TES algorithm (*Worden et al.*, 2004, 2012). AIRS and OMI radiances are combined following the methods in Sec. 3.4 and described in detail in *Fu et al.* (2018). The uncertainties and degrees of freedom for signal (DOFS) of the combined AIRS/OMI O_3 is similar to that of TES. Performance related to CrIS and TROPOMI will be considered in a future version.

3.5.3 Carbon Monoxide (CO)

Atmospheric carbon monoxide (CO) can be measured by remote sensing using molecular absorption lines in the thermal infrared (TIR, around 4.6 μm) and the shortwave infrared (SWIR, around 2.3 μm). AIRS and CrIS both provide TIR observations that are sensitive to CO in the middle troposphere with limited vertical information, around 1-2 DOFS. TROPOMI SWIR observations (to be considered in future releases) rely on reflected solar radiation and are sensitive to the total column of CO, but without vertical information ($\sim$1 DOFS). *Fu et al.* (2016) describes the algorithms and simulated results for CrIS (TIR) and TROPOMI (SWIR) separately and for multispectral retrievals. Multispectral retrievals allow enhanced sensitivity to near-surface CO by combining the CO total column (SWIR) with free tropospheric vertical CO profile information from TIR observations.

3.5.4 Ammonia (NH_3)

The NH_3 algorithm is described in *Shephard and Cady-Pereira* (2015). The algorithm uses the NH_3 feature at 967 cm^{-1} to estimate NH_3 profiles. The constraint is set by the initial brightness temperature in the active spectral region, and the initial guess is always the same. The temperature, water, and surface temperature are set from GMAO values and emissivity is set from a MODIS-derived database (*Seemann et al.*, 2008). Over regions with measurable concentrations (greater than 0.5 ppbv) the Degrees of Freedom for Signal (DOFS) are on the order of 0.9. Validation of the Environment Canada implementation of this algorithm (*Dammers et al.*, 2017) showed a small negative bias (0-10%) at high concentrations and a significant positive bias (as large as 50%) for low concentrations (less than 1.0 ppbv).

3.5.5 Deuterated Water (HDO)

The algorithm to quantify the HDO/H_2O ratio of tropospheric water vapor is first described in *Worden et al.* (2006) and then updated for the AIRS and CrIS retrievals in *Worden et al.* (2019). The retrieval approach is to quantify HDO, H_2O, and other geophysical parameters affecting the observed radiance (e.g., temperature, methane, emissivity) using the measured radiances from the 8 through 12 micron bands. The validation of the AIRS measurements are reported in *Herman et al.* (2020) and show that calculated uncertainties of 30 parts per thousand relative to the deuterium content of ocean water (or SMOW) for an integrated quantity between 850 hPa and 350 hPa is consistent with tropical aircraft data that approximately overlap the AIRS measurements. The CrIS and AIRS measurements agree to within their reported uncertainties.

3.5.6 Methane (CH_4)

The algorithm for retrievals of CH_4 from single footprint AIRS radiances is described in *Worden et al.* (2012, 2019). Validation of AIRS CH_4 against reference aircraft profiles is described in *Kulawik et al.* (2021). The algorithm for CrIS CH_4 retrievals follows the same approach.

3.5.7 Peroxyacetyl Nitrate (PAN)

PAN is currently retrieved from CrIS radiances using the PAN feature centered around 790 cm^{-1}. CrIS PAN retrievals have been validated using in situ aircraft profiles from the ATom aircraft campaigns (*Wofsy et al.*, 2018). The CrIS PAN algorithm and the ATom comparisons are described in *Payne et al.* (submitted). CrIS observations of PAN in wildfire plumes over the Western US during the WE-CAN campaign period, including comparisons of PAN/CO enhancement ratios from CrIS with those measured from aircraft, have been analyzed by *Calahorrano et al.* (submitted).

3.6 Error Analysis

Optimal estimation provides a rich set of tools to assess the uncertainty in the retrieval, $\hat{\mathbf{x}} = \mathbf{M}\hat{\mathbf{z}}$. If the minimum calculated in Eq. 5 is sufficiently close to the solution under moderately nonlinear conditions (*Rodgers*, 2000), then the relationship between the estimated and the true state can approximated by a linear solution (*Bowman et al.*, 2006):

$$\hat{\mathbf{x}} = \mathbf{x}_a + \mathbf{A}_{xx}(\mathbf{x} - \mathbf{x}_a) + \varepsilon_r + \varepsilon_{cs} \tag{6}$$

where $\hat{\mathbf{x}}$ is the retrieval from Eq. 5, $\mathbf{x}_a$ is the a priori state vector in Eq. 4 and $\mathbf{A}_{xx}$ is the averaging kernel. The averaging kernel describes the sensitivity of the estimate to the true state:

$$\mathbf{A}_{xx} = \frac{\partial \hat{\mathbf{x}}}{\partial \mathbf{x}}. \tag{7}$$

The subscript xx refers to the sensitivity calculated on the full state vector. The averaging kernel can also be calculated on the retrieval grid, $\mathbf{z}$. A key diagnostic is the degrees of freedom for signal (dofs)(*Rodgers*, 2000)

$$\text{dofs} = \text{Tr}(\mathbf{A}_{xx}). \tag{8}$$

Degrees of freedom for signal is a measure of the number of independent pieces of information provided by the measurement, weighted according to the signal-to-noise variance of each piece of information.

There are two sources of error. The first is the propagation of measurement noise into the retrieval:

$$\varepsilon_r = \mathbf{M}\mathbf{G}_z\varepsilon \tag{9}$$

where $\mathbf{M}$ is the mapping matrix defined in Eq. 3, $\mathbf{G}_z$ is the gain matrix (*Bowman et al.*, 2006), and ε is the random noise defined in Eq. 2. The second source of error in the "cross-state" error:

$$\varepsilon_{cs} = \sum_i \mathbf{M}\mathbf{G}_z\mathbf{K}_b^i(\mathbf{b}^i - \mathbf{b}_a^i) \tag{10}$$

where $\mathbf{b}_i$ is a non-retrieved quantity, $\mathbf{b}_a$ is the prior, $\mathbf{K}_b^i$ is the Jacobian of the non-retrieved vector, $\mathbf{b}_i$. The vector $\mathbf{b}$ is often an atmospheric state vector retrieved in a previous step. For example, temperature and water vapor can be retrieved before, say, PAN or NH_3. While they may not be retrieved, they are still uncertain. Consequently, that quantity will propagate into the subsequent retrieval.

The error in the retrieval can be written as

$$\tilde{\mathbf{x}} = \hat{\mathbf{x}} - \mathbf{x}. \tag{11}$$

The statistics of the error can be computed from Eq. 6 as

$$\mathbf{S}_{\tilde{\mathbf{x}}} = \mathbf{S}_s + \mathbf{S}_{obs}. \tag{12}$$

The smoothing error, $\mathbf{S}_s$, is defined as

$$\mathbf{S}_s = (\mathbf{I} - \mathbf{A}_{xx})\mathbf{S}_x(\mathbf{I} - \mathbf{A}_{xx})^\top \tag{13}$$

where $\mathbf{S}_x$ is the uncertainty of the true state, which we take as the a prior uncertainty. The observational error, $\mathbf{S}_{obs}$, combines the random, cross-state, and systematic error covariance matrices. The interested reader is referred to Eqs. 42-45 in *Bowman et al.* (2006) for additional details.

3.7 Observation operator

The methods developed in Sec. 3.6 provide important tools to ingest retrievals into downstream data assimilation systems and facilitate comparisons with other instruments or in-situ data. We use these to construct an observation operator, which project an atmospheric state to a "virtual" retrieval, i.e., what a retrieval would look like for a given true state. The observation operator is represented as (*Jones et al.*, 2003)

$$\mathbf{H}(\cdot) = \mathbf{x}_a + \mathbf{A}_{xx}(\cdot - \mathbf{x}_a). \tag{14}$$

The use of the observation operator in chemical data assimilation is illustrated in Fig. 3. The retrieval system minimizes the cost function in Eq. 4 to estimate an atmospheric state given an observed radiance, $\mathbf{y}$. The linearized relationship between the true state and the retrieved state (Eq. 6) becomes the basis for the observation operator (Eq. 14), which is constructed from Eq. 6. This operator is passed to the chemical data assimilation system. Mathematically, these systems solve the same problem as the retrieval problem. Spatio-temporal distribution of observations–the retrievals–are compared to predicted fields and the model control vector is modified to minimize those differences subject to background statistics of the global distribution (e.g., *Bowman et al.*, 2017; *Miyazaki et al.*, 2020a,b).

In addition to data assimilation, observation operators are used to compare to in-situ data such as ozonesondes (e.g., *Nassar et al.*, 2008; *Worden et al.*, 2007a), comparison to chemistry-climate models (e.g. *Aghedo et al.*, 2011; *Miyazaki and Bowman*, 2017) as well as other instruments (e.g., *Luo et al.*, 2007; *Rodgers and Connor*, 2003).

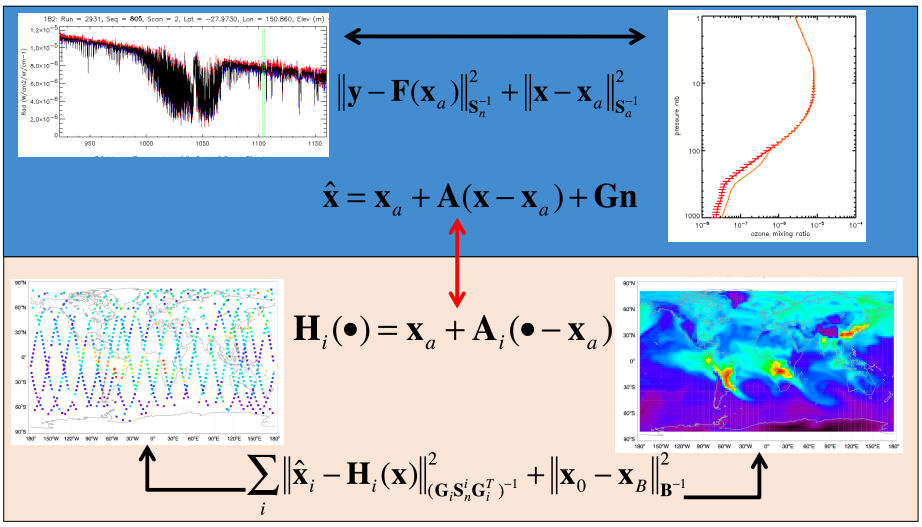

Fig. 3. Use of the observation operator in data assimilation. The top panel is a geophysical retrieval from a spectrum. The a priori and averaging kernels are used to construct the observation operator. This operator is passed to the chemical data assimilation system.

References

Aghedo, A. M., K. W. Bowman, D. T. Shindell, and G. Faluvegi (2011), The impact of orbital sampling, monthly averaging and vertical resolution on climate chemistry model evaluation with satellite observations, *Atmos. Chem. Phys.*, *11*(13), 6493–6514, doi:10.5194/acp-11-6493-2011.

Bak, J., X. Liu, J.-H. Kim, D. P. Haffner, K. Chance, K. Yang, and K. Sun (2017), Characterization and correction of omps nadir mapper measurements for ozone profile retrievals, *10*(11), 4373–4388, doi:10.5194/amt-10-4373-2017.

Beer, R. (1992), *Remote Sensing by Fourier Transform Spectrometry*, John Wiley & Sons, New York, London, Sydney.

Beer, R. (2006), TES on the Aura mission: Scientific objectives, measurements, and analysis overview, *IEEE Trans. on Geosci. Remote Sensing*, *44*(5), 1102–1105.

Bowman, K. W., H. M. Worden, and R. Beer (2000), Instrument Line-Shape Modeling and Correction for Off-Axis Detectors in Fourier-Transform Spectrometry, *Appl. Opt.*, *39*(21), 3765–3773.

Bowman, K. W., C. D. Rodgers, S. S. Kulawik, J. Worden, E. Sarkissian, G. Osterman, T. Steck, M. Lou, A. Eldering, M. Shephard, H. Worden, M. Lampel, S. Clough, P. Brown, C. Rinsland, M. Gunson, and R. Beer (2006), Tropospheric emission spectrometer: Retrieval method and error analysis, *IEEE Trans. on Geosci. Remote Sensing*, *44*(5), doi:10.1109/TGRS.2006.871234.

Bowman, K. W., J. Liu, A. A. Bloom, N. C. Parazoo, M. Lee, Z. Jiang, D. Menemenlis, M. M. Gierach, G. J. Collatz, K. R. Gurney, and D. Wunch (2017), Global and Brazilian carbon response to El Niño Modoki 2011-2010, *Earth and Space Science*, *4*, doi:10.1002/2016EA000204.

Brion, J., A. Chakir, D. Daumont, J. Malicet, and C. Parisse (1993), High-resolution laboratory absorption cross section of o3. temperature effect, *213*(5-6), 610–612, doi:10.1016/0009-2614(93)89169-i.

Calahorrano, J., V. H. Payne, S. S. Kulaiwk, F. F. T. Campos, and E. . Fischer (submitted), Evolution of wildfire smoke plumes detected by the Cross-trach Infrared Sounder (CrIS) over the western US during summer 2018, *Geophys. Res. Lett*.

Clough, S., M. Shepard, J. R. Worden, P. D. Brown, H. M. Worden, M. Lou, C. Rodgers, C. Rinsland, A. Goldman, L. Brown, A. Eldering, S. S. Kulawik, K. Cady-Pereira, G. Osterman, and R. Beer (2006), Forward Model and Jacobians for Tropospheric Emission Spectrometer Retrievals, *IEEE Transactions on Geoscience and Remote Sensing*, *44*(5), 1308–1323.

Dammers, E., M. W. Shephard, M. Palm, K. Cady-Pereira, S. Capps, E. Lutsch, K. Strong, J. W. Hannigan, I. Ortega, G. C. Toon, W. Stremme, M. Grutter, N. Jones, D. Smale, J. Siemons, K. Hrpcek, D. Tremblay, M. Schaap, J. Notholt, and J. W. Erisman (2017), Validation of the cris fast physical nh3 retrieval with ground-based ftir, *10*(7), 2645–2667, doi:10.5194/amt-10-2645-2017.

Duan, M., Q. Min, and J. Li (2005), A fast radiative transfer model for simulating high-

resolution absorption bands, *110*(D15), doi:10.1029/2004jd005590.

Eldering, A., S. S. Kulawik, J. Worden, K. Bowman, and G. Osterman (2008), Implementation of cloud retrievals for TES atmospheric retrievals: 2. Characterization of cloud top pressure and effective optical depth retrievals, *J. Geophys. Res.*, *113*, D16S37, doi:10.1029/2007JD008858.

Fu, D., J. R. Worden, X. Liu, S. S. Kulawik, K. W. Bowman, and V. Natraj (2013), Characterization of ozone profiles derived from Aura TES and OMI radiances, *Atmos. Chem. Phys.*, *13*(6), 3445–3462, doi:10.5194/acp-13-3445-2013.

Fu, D., K. W. Bowman, H. M. Worden, V. Natraj, J. R. Worden, S. Yu, P. Veefkind, I. Aben, J. Landgraf, L. Strow, and Y. Han (2016), High-resolution tropospheric carbon monoxide profiles retrieved from CrIS and TROPOMI, *Atmos. Meas. Tech.*, *9*(6), 2567–2579, doi:10.5194/amt-9-2567-2016.

Fu, D., S. S. Kulawik, K. Miyazaki, K. W. Bowman, J. R. Worden, A. Eldering, N. J. Livesey, J. Teixeira, F. W. Irion, R. L. Herman, G. B. Osterman, X. Liu, P. F. Levelt, A. M. Thompson, and M. Luo (2018), Retrievals of tropospheric ozone profiles from the synergism of AIRS and OMI: methodology and validation, *Atmos. Meas. Tech.*, *11*(10), 5587–5605, doi:10.5194/amt-11-5587-2018.

Gelaro, R., W. McCarty, M. J. Suárez, R. Todling, A. Molod, L. Takacs, C. A. Randles, A. Darmenov, M. G. Bosilovich, R. Reichle, K. Wargan, L. Coy, R. Cullather, C. Draper, S. Akella, V. Buchard, A. Conaty, A. M. da Silva, W. Gu, G.-K. Kim, R. Koster, R. Lucchesi, D. Merkova, J. E. Nielsen, G. Partyka, S. Pawson, W. Putman, M. Rienecker, S. D. Schubert, M. Sienkiewicz, and B. Zhao (2017), The Modern-Era Retrospective Analysis for Research and Applications, Version 2 (MERRA-2), *Journal of Climate*, *30*(14), 5419–5454, doi:10.1175/JCLI-D-16-0758.1.

Herman, R. L., J. Worden, D. Noone, D. Henze, K. Bowman, K. Cady-Pereira, V. H. Payne, S. S. Kulawik, and D. Fu (2020), Comparison of optimal estimation HDO/H_2O retrievals from AIRS with ORACLES measurements, *Atmospheric Measurement Techniques*, *13*(4), 1825–1834, doi:10.5194/amt-13-1825-2020.

Jones, D. B. A., K. W. Bowman, P. I. Palmer, J. R. Worden, D. J. Jacob, R. N. Hoffman, I. Bey, and R. M. Yantosca (2003), Potential of observations from the Tropospheric Emission Spectrometer to constrain continental sources of carbon monoxide, *J. Geophys. Res.-Atmospheres*, *108*(D24), 4789, doi:doi:10.1029/2003JD003702.

Kleipool, Q. L., M. R. Dobber, J. F. d. Haan, and P. F. Levelt (2008), Earth surface reflectance climatology from 3 years of omi data, *113*(D18), doi:10.1029/2008jd010290.

Kopparla, P., V. Natraj, R. Spurr, R.-L. Shia, D. Crisp, and Y. L. Yung (2016), A fast and accurate pca based radiative transfer model: Extension to the broadband shortwave region, *173*, 65–71, doi:10.1016/j.jqsrt.2016.01.014.

Kopparla, P., V. Natraj, D. Limpasuvan, R. Spurr, D. Crisp, R.-L. Shia, P. Somkuti, and Y. L. Yung (2017), Pca-based radiative transfer: Improvements to aerosol scheme, vertical layering and spectral binning, *198*, 104–111, doi:10.1016/j.jqsrt.2017.05.005.

Kulawik, S. S., J. Worden, A. Eldering, K. Bowman, M. Gunson, G. B. Osterman, L. Zhang, S. A. Clough, M. W. Shephard, and R. Beer (2006a), Implementation of cloud

retrievals for Tropospheric Emission Spectrometer (TES) atmospheric retrievals: Part 1. Description and characterization of errors on trace gas retrievals, *J. Geophys. Res.*, *111*(D24).

Kulawik, S. S., H. Worden, G. Osterman, M. Luo, R. Beer, D. E. Kinnison, K. W. Bowman, J. Worden, A. Eldering, M. Lampel, T. Steck, and C. D. Rodgers (2006b), TES atmospheric profile retrieval characterization: an orbit of simulated observations, *IEEE Transactions on Geoscience and Remote Sensing*, *44*(5), 1324–1333, doi:10.1109/TGRS.2006.871207.

Kulawik, S. S., J. R. Worden, V. H. Payne, D. Fu, S. C. Wofsy, K. McKain, C. Sweeney, B. C. D. Jr., A. Lipton, I. Polonsky, Y. He, K. E. Cady-Pereira, E. J. Dlugokencky, D. J. Jacob, and Y. Yin (2021), Evaluation of single-footprint AIRS CH4 profile retrieval uncertainties using aircraft profile measurements, *Atmospheric Measurement Techniques*, *14*(1), 335–354, doi:10.5194/amt-14-335-2021.

Lee, R. A. M., C. W. O'Dell, D. Wunch, C. M. Roehl, G. B. Osterman, J. Blavier, R. Rosenberg, L. Chapsky, C. Frankenberg, S. L. Hunyadi-Lay, B. M. Fisher, D. M. Rider, D. Crisp, and R. Pollock (2017), Preflight Spectral Calibration of the Orbiting Carbon Observatory 2, *IEEE Transactions on Geoscience and Remote Sensing*, *55*(5), 2499–2508, doi:10.1109/TGRS.2016.2645614.

Liu, X., K. Chance, C. E. Sioris, and T. P. Kurosu (2007), Impact of using different ozone cross sections on ozone profile retrievals from global ozone monitoring experiment (gome) ultraviolet measurements, *7*(13), 3571–3578, doi:10.5194/acp-7-3571-2007.

Liu, X., P. K. Bhartia, K. Chance, R. J. D. Spurr, and T. P. Kurosu (2010a), Ozone profile retrievals from the ozone monitoring instrument, *Atmos. Chem. Phys.*, *10*(5), 2521–2537, doi:10.5194/acp-10-2521-2010.

Liu, X., P. K. Bhartia, K. Chance, L. Froidevaux, R. J. D. Spurr, and T. P. Kurosu (2010b), Validation of Ozone Monitoring Instrument (OMI) ozone profiles and stratospheric ozone columns with Microwave Limb Sounder (MLS) measurements, *Atmos. Chem. Phys.*, *10*(5), 2539–2549.

Luo, M., C. P. Rinsland, C. D. Rodgers, J. A. Logan, H. Worden, S. Kulawik, A. Eldering, A. Goldman, M. W. Shephard, M. Gunson, and M. Lampel (2007), Comparison of carbon monoxide measurements by TES and MOPITT – the influence of a priori data and instrument characteristics on nadir atmospheric species retrievals, *J. Geophys. Res.-Atmospheres*, D09303, doi:10.1029/2006JD007663.

Miyazaki, K., and K. Bowman (2017), Evaluation of ACCMIP ozone simulations and ozonesonde sampling biases using a satellite-based multi-constituent chemical reanalysis, *Atmos. Chem. Phys.*, *17*(13), 8285–8312, doi:10.5194/acp-17-8285-2017.

Miyazaki, K., K. Bowman, T. Sekiya, H. Eskes, F. Boersma, H. Worden, N. Livesey, V. H. Payne, K. Sudo, Y. Kanaya, M. Takigawa, and K. Ogochi (2020a), Updated tropospheric chemistry reanalysis and emission estimates, TCR-2, for 2005–2018, *Earth System Science Data*, *12*(3), 2223–2259, doi:10.5194/essd-12-2223-2020.

Miyazaki, K., K. W. Bowman, K. Yumimoto, T. Walker, and K. Sudo (2020b), Evaluation of a multi-model, multi-constituent assimilation framework for tropospheric chemical

reanalysis, *Atmos. Chem. Phys.*, *20*(2), 931–967, doi:10.5194/acp-20-931-2020.

Moncet, J.-L., G. Uymin, A. E. Lipton, and H. E. Snell (2008), Infrared radiance modeling by optimal spectral sampling, *Journal of the Atmospheric Sciences*, *65*(12), 3917–3934.

Moncet, J.-L., G. Uymin, P. Liang, and A. E. Lipton (2015), Fast and accurate radiative transfer in the thermal regime by simultaneous optimal spectral sampling over all channels, *Journal of the Atmospheric Sciences*, *72*(7), 2622–2641, doi:10.1175/JAS-D-14-0190.1.

Nassar, R., J. Logan, H. Worden, I. A. Megretskaia, K. Bowman, G. Osterman, A. M. Thompson, D. W. Tarasick, S. Austin, H. Claude, M. K. Dubey, W. K. Hocking, B. J. Johnson, E. Joseph, J. Merrill, G. A. Morris, M. Newchurch, S. J. Oltmans, F. Posny, and F. Schmidlin (2008), Validation of Tropospheric Emission Spectrometer (TES) Nadir Ozone Profiles Using Ozonesonde Measurements, *J. Geophys. Res*, *113*, D15S17, doi:10.1029/2007JD008819,.

Natraj, V., X. Jiang, R.-l. Shia, X. Huang, J. S. Margolis, and Y. L. Yung (2005), Application of principal component analysis to high spectral resolution radiative transfer: A case study of the o2 a band, *95*(4), 539–556, doi:10.1016/j.jqsrt.2004.12.024.

Natraj, V., R.-L. Shia, and Y. L. Yung (2010), On the use of principal component analysis to speed up radiative transfer calculations, *111*(5), 810–816, doi:10.1016/j.jqsrt.2009.11.004.

Payne, V. H., S. S. Kulaiwk, E. V. Fischer, J. Brewer, L. G. Huey, K. Miyazaki, J. R. Worden, K. W. Bowman, S. Wofsy, J. Elkins, E. Hintsa, and F. Moore (submitted), Satellite measurements of peroxyacetyl nitrate from the Cross-track. Infrared Sounder: Comparisons with ATom aircraft measurements, *Atmos. Meas. Tech*.

Rodgers, C. (2000), *Inverse Methods for Atmospheric Sounding: Theory and Practise*, World Scientific, London.

Rodgers, C., and B. Connor (2003), Intercomparison of remote sounding instruments, *J. Geophys. Res.*, *108(D3)*, 4119.

Seemann, S. W., E. E. Borbas, R. O. Knuteson, G. R. Stephenson, and H.-L. Huang (2008), Development of a global infrared land surface emissivity database for application to clear sky sounding retrievals from multispectral satellite radiance measurements, *Journal of Applied Meteorology and Climatology*, *47*(1), 108–123, doi:10.1175/2007JAMC1590.1.

Shephard, M. W., and K. E. Cady-Pereira (2015), Cross-track Infrared Sounder (CrIS) satellite observations of tropospheric ammonia, *Atmos. Meas. Tech.*, *8*(3), 1323–1336, doi:10.5194/amt-8-1323-2015.

Sioris, C. E., and W. F. J. Evans (2000), Impact of rotational raman scattering in the o2a band, *27*(24), 4085–4088, doi:10.1029/2000gl012231.

Spurr, R. (2008), Light scattering reviews 3, light scattering and reflection, pp. 229–275, doi:10.1007/978-3-540-48546-9{_}7.

Spurr, R., and V. Natraj (2011), A linearized two-stream radiative transfer code for fast approximation of multiple-scatter fields, *112*(16), 26302,637, doi:10.1016/j.jqsrt.2011.06.014.

Spurr, R., V. Natraj, C. Lerot, M. V. Roozendael, and D. Loyola (2013), Linearization of the

principal component analysis method for radiative transfer acceleration: Application to retrieval algorithms and sensitivity studies, *125*, 1–17, doi:10.1016/j.jqsrt.2013.04.002.

Spurr, R. J. D. (2006), Vlidort: A linearized pseudo-spherical vector discrete ordinate radiative transfer code for forward model and retrieval studies in multilayer multiple scattering media, *102*(2), 316–342, doi:10.1016/j.jqsrt.2006.05.005.

Tarantola, A. (2005), *Inverse Problem Theory: Methods for Data Fitting and Model Parameter Estimation*, SIAM.

Wofsy, S. C., S. Afshar, H. M. Allen, E. C. Apel, E. C. Asher, B. Barletta, J. Bent, H. Bian, B. C. Biggs, D. R. Blake, N. Blake, I. Bourgeois, C. A. Brock, W. H. Brune, J. W. Budney, T. P. Bui, A. Butler, P. Campuzano-Jost, C. S. Chang, M. Chin, R. Commane, G. Correa, J. D. Crounse, P. D. Cullis, B. C. Daube, D. A. Day, J. M. Dean-Day, J. E. Dibb, J. P. DiGangi, G. S. Diskin, M. Dollner, J. W. Elkins, F. Erdesz, A. M. Fiore, C. M. Flynn, K. D. Froyd, D. W. Gesler, S. R. Hall, T. F. Hanisco, R. A. Hannun, A. J. Hills, E. J. Hintsa, A. Hoffman, R. S. Hornbrook, L. G. Huey, S. Hughes, J. L. Jimenez, B. J. Johnson, J. M. Katich, R. F. Keeling, M. J. Kim, A. Kupc, L. R. Lait, J. F. Lamarque, J. Liu, K. McKain, R. J. Mclaughlin, S. Meinardi, D. O. Miller, S. A. Montzka, F. L. Moore, E. J. Morgan, D. M. Murphy, L. T. Murray, B. A. Nault, J. A. Neuman, P. A. Newman, J. M. Nicely, X. Pan, W. Paplawsky, J. Peischl, M. J. Prather, D. J. Price, E. A. Ray, J. M. Reeves, M. Richardson, A. W. Rollins, K. H. Rosenlof, T. B. Ryerson, E. Scheuer, G. P. Schill, J. C. Schroder, J. P. Schwarz, J. M. St. Clair, S. D. Steenrod, B. B. Stephens, S. A. Strode, C. Sweeney, D. Tanner, A. P. Teng, A. B. Thames, C. R. Thompson, K. Ullmann, P. R. Veres, N. Vieznor, N. L. Wagner, A. Watt, R. Weber, B. Weinzierl, P. O. Wennberg, C. J. Williamson, J. C. Wilson, G. M. Wolfe, C. T. Woods, and L. H. Zeng (2018), ATom: Merged Atmospheric Chemistry, Trace Gases, and Aerosols, doi:10.3334/ORNLDAAC/1581.

Worden, H. M., J. A. Logan, J. R. Worden, R. Beer, K. Bowman, S. A. Clough, A. Eldering, B. M. Fisher, M. R. Gunson, R. L. Herman, S. S. Kulawik, M. C. Lampel, M. Luo, I. A. Megretskaia, G. B. Osterman, and M. W. Shephard (2007a), Comparisons of Tropospheric Emission Spectrometer (TES) ozone profiles to ozonesondes: Methods and initial results, *Journal of Geophysical Research: Atmospheres*, *112*(D3), doi:10.1029/2006jd007258.

Worden, J., S. S. Kulawik, M. W. Shephard, S. A. Clough, H. Worden, K. Bowman, and A. Goldman (2004), Predicted errors of tropospheric emission spectrometer nadir retrievals from spectral window selection, *Journal of Geophysical Research: Atmospheres*, *109*(D9), doi:10.1029/2004JD004522.

Worden, J., K. Bowman, D. Noone, R. Beer, S. Clough, A. Eldering, B. Fisher, A. Goldman, M. Gunson, R. Herman, S. S. Kulawik, M. Lampel, M. Lou, G. B. Osterman, C. Rinsland, C. Rodgers, S. P. Sander, M. Shephard, and H. Worden (2006), Tropospheric Emission Spectrometer observations of the tropospheric HDO/H2O ratio: Estimation approach and characterization, *J. Geophys. Res.*, *111*, D16309, doi:10.1029/2005JD006606.

Worden, J., X. Liu, K. Bowman, K. Chance, R. Beer, A. Eldering, M. Gunson, and H. Wor-

den (2007b), Improved tropospheric ozone profile retrievals using OMI and TES radiances, *Geophys. Res. Lett.*, *34*, L01809, doi:10.1029/2006GL027806.

Worden, J., S. Kulawik, C. Frankenberg, V. Payne, K. Bowman, K. Cady-Peirara, K. Wecht, J. E. Lee, and D. Noone (2012), Profiles of CH4, HDO, H2O, and N2O with improved lower tropospheric vertical resolution from Aura TES radiances, *Atmos. Meas. Tech.*, *5*(2), 397–411, doi:10.5194/amt-5-397-2012.

Worden, J. R., S. S. Kulawik, D. Fu, V. H. Payne, A. E. Lipton, I. Polonsky, Y. He, K. Cady-Pereira, J.-L. Moncet, R. L. Herman, F. W. Irion, and K. W. Bowman (2019), Characterization and evaluation of airs-based estimates of the deuterium content of water vapor, *Atmospheric Measurement Techniques*, *12*(4), 2331–2339, doi: 10.5194/amt-12-2331-2019.